Drug Design, Development and Therapy

Dovepress
Taylor & Francis Group

Open Access Full Text Article

ORIGINAL RESEARCH

Canagliflozin as a Potential Preclinical Therapy for Tuberous Sclerosis Complex: Inhibition of *Tsc2*$^{-/-}$ Cell Proliferation via Cell Cycle Arrest and Mitochondrial Dysfunction

Juan Ye[1,2,*], Boyuan Liu[3,*], Jing Wu[4,*], Hongliang Gao[5], Qingyun Wei[2], Kelei Su[2], Kai Zheng[6], Xuening Dai[3], Tao Xu[3], Yuqi Wang[3], Shuangchi Liu[7], Xing Peng[3], Liming Gou[4], Yinjuan Zhao[8,*], Bin Xue[1,4,7,9,10]

[1]Medical School, Nanjing University Nanjing, Jiangsu, 210023, People's Republic of China; [2]Affiliated Hospital of Integrated Traditional Chinese and Western Medicine, Nanjing University of Chinese Medicine, Nanjing, Jiangsu, 210028, People's Republic of China; [3]Sir Run Run Hospital, Nanjing Medical University, Nanjing, Jiangsu, 211166, People's Republic of China; [4]Translational Medicine Research Center, Children's Hospital of Nanjing Medical University, Nanjing, 210000, People's Republic of China; [5]Department of Pathophysiology, Wannan Medical college, Wuhu, 241002,People's Republic of China; [6]Jiangsu Province Engineering Research Center of Stomatological Translational Medicine, Affiliated Hospital of Stomatology, Nanjing Medical University, Nanjing, 210029, People's Republic of China; [7]Department of General Surgery, the Affiliated Changzhou Second People's Hospital of Nanjing Medical University, Changzhou, 213003, People's Republic of China; [8]Collaborative Innovation Center of Sustainable Forestry in Southern China, College of Forestry, Nanjing Forestry University, Nanjing, 210037, People's Republic of China; [9]NHC Key Laboratory of Antibody Technique, Nanjing Medical University, Nanjing, People's Republic of China; [10]Collaborative Innovation Center for Cancer Personalized Medicine, Nanjing Medical University, Nanjing, 211166, People's Republic of China

*These authors contributed equally to this work: Juan Ye, Boyuan Liu, Jing Wu

Correspondence: Bin Xue; Yinjuan Zhao, Email xuebin@njmu.edu.cn; zhaoyinjuan@njfu.edu.cn

Purpose: Canagliflozin (Ca), a sodium-glucose cotransporter 2 (SGLT2) inhibitor traditionally used for type 2 diabetes, has shown potential in the treatment of lymphangiomatosis (the pulmonary lesion phenotype of TSC). However, its effects on *Tsc2*$^{-/-}$ cells, a key feature of tuberous sclerosis complex (TSC), have not been previously explored. This preclinical study aimed to investigate Ca's inhibitory mechanisms on *Tsc2*$^{-/-}$ cell proliferation and its therapeutic potential in TSC-related lesions.

Methods: The effects of Ca on *Tsc2*$^{-/-}$ cells were evaluated using in vitro cellular assays, including proliferation, cell cycle, and mitochondrial function analyses, as well as proteomics. In vivo, a mouse xenograft model was employed to assess tumor growth inhibition and safety profile. Comparative studies with other SGLT2 inhibitors were conducted to identify compound-specific mechanisms.

Results: Ca significantly inhibited *Tsc2*$^{-/-}$ cell proliferation in a dose-dependent manner, inducing G1 phase cell cycle arrest and impairing mitochondrial function, as evidenced by reduced membrane potential and ATP production. Proteomic analysis revealed mitochondrial protein alterations, and Ca-induced ROS accumulation promoted apoptosis. In vivo, Ca (100 mg/kg/day) effectively suppressed tumor growth without significant adverse effects. Notably, Ca's effects were unique compared to other SGLT2 inhibitors, indicating mechanisms independent of SGLT2 inhibition.

Conclusion: Ca inhibits *Tsc2*$^{-/-}$ cell proliferation through dual mechanisms of cell cycle arrest and mitochondrial impairment, demonstrating significant therapeutic potential for TSC-related lesions. These findings highlight Ca as a promising alternative to current mTOR inhibitors, warranting further investigation into its molecular targets and clinical applications.

Keywords: canagliflozin, rare diseases, mitochondrial impairment, *Tsc2* gene

Introduction

Tuberous sclerosis complex 2 (TSC2) is a critical tumor suppressor gene located on human chromosome 16p13.3. It encodes tuberin, a protein that forms a complex with the TSC1 gene product, hamartin, to co-regulate the mammalian target of rapamycin complex 1 (mTORC1) signaling pathway.[1] This complex exerts its regulatory function by inhibiting

Received: 31 March 2025
Accepted: 24 November 2025
Published: 4 December 2025

the activity of the GTPase Rheb, a key activator of mTORC1, thereby controlling essential biological processes such as cell growth, proliferation, metabolism, and autophagy.[2] Loss-of-function mutations in TSC2—such as point mutations, exon deletions, or rearrangements—lead to the overactivation of the mTOR pathway.[1,3] This disorder drives abnormal cell proliferation and leads to the occurrence of tuberous sclerosis complex (TSC).[4]

TSC is an autosomal dominant inherited neurocutaneous syndrome, and there are also sporadic cases. It is mostly caused by abnormal organ development in the ectodermal tissue. The clinical features include facial sebaceous adenoma, epileptic seizures and intellectual decline.[5] In addition, depending on the affected area, patients may also develop secondary retinal glioma, renal angiomyolipoma (AML), cardiac rhabdomytoma and pulmonary lymphangiomytomatosis (LAM), etc.[5]

Although mTOR inhibitors (such as rapamycin and its analogues) have clinical benefits, there are still significant challenges in the treatment of TSC-related diseases. Firstly, mTOR inhibition usually leads to incomplete inhibition of disease progression, as demonstrated by the recurrence of tumors and lung lesions after treatment discontinuation.[6] Secondly, long-term use of mTOR inhibitors is associated with significant side effects, including immunosuppression, hyperlipidemia and impaired wound healing, which limits their therapeutic window and patient compliance.[7] Thirdly, mTOR inhibitors mainly target mTORC1, keeping the mTORC2 signaling intact, which may contribute to the compensatory mechanisms for drug resistance and disease progression.[8] These limitations emphasize the urgent need for new therapeutic strategies to address TSC2-related diseases.

Sodium-glucose cotransporter 2 (SGLT2) inhibitors, originally developed as oral agents for the treatment of type 2 diabetes mellitus (T2DM), reduce glucose reabsorption in the proximal tubules of the kidney, thereby lowering blood glucose levels without impairing renal function.[9] Beyond their primary hypoglycemic effects, SGLT2 inhibitors exhibit multiple pleiotropic properties that favorably influence cardiovascular disease outcomes.[10]

Among SGLT2 inhibitors, Canagliflozin (Ca) is increasingly being used in the treatment of various other diseases due to its superior anti-inflammatory, anti-cancer and organ-protective properties. Ca has been proven to exert anti-inflammatory effects by reducing glucose uptake by macrophages and decreasing the production and release of inflammatory factors induced by lipopolysaccharides.[11] Ca can also mediate the tumor suppressive effect of non-small cell lung cancer (NSCLC) alone by inhibiting HIF-1α and in combination with radiotherapy.[12] Recently, some researchers have designed a universal nano-liposome coated with PD-L1-targeting peptides to efficiently deliver Ca in vivo. This simply prepared nanomedicine exhibits specific tumor-targeting ability and excellent biosafety.[13] Furthermore, Ca has been identified as a novel inhibitor of the proliferation and migration of vascular smooth muscle cells. Studies have shown that Ca stimulates the expression of heme oxygenase-1 (HO-1) in vascular smooth muscle cells through the ROS-Nrf2 pathway, and this induction of HO-1 contributes to its cellular effect.[14] Abnormal proliferation of vascular smooth muscle cells is precisely the clinical manifestation of TSC in pulmonary lesions. In addition, studies have shown that Ca significantly alleviates cardiac dysfunction and improves mitochondrial function both in vitro and in vivo.[15]

Direct studies on mitochondrial dysfunction in TSC are relatively few, but existing research has shown that mitochondrial dysfunction can lead to insufficient ATP production in neurons, intensifying the frequency of epileptic seizures and brain injury.[16] Meanwhile, the imbalance of mitochondrial calcium ion regulation may induce calcium overload, promote neuroexcitotoxicity and accelerate the decline of cognitive function.[17] Furthermore, mitochondrial dysfunction can trigger excessive accumulation of reactive oxygen species (ROS), leading to oxidative stress. In TSC, ROS can activate inflammatory pathways (such as NF-κB and NLRP3 inflammasomes), promote microglial activation and neuroinflammation, and aggravate demyelination and axonal injury around cortical nodules.[18] Although the pathogenic core of TSC is the excessive activation of the mTOR pathway caused by mutations in the TSC1/TSC2 genes, mitochondrial dysfunction may accelerate multi-organ lesions (especially neurodegeneration and the progression of epilepsy) through energy crises, oxidative stress and apoptotic signals. Future protection strategies for mitochondria may provide a new direction for the adjuvant treatment of TSC.

In this preclinical study, we investigate the anti-proliferative effects of Ca on $Tsc2^{-/-}$ cells both in vitro and in vivo, with a focus on its impact on cell cycle regulation and mitochondrial function. Utilizing proteomic analysis, we identify key molecular targets and pathways modulated by Ca, providing mechanistic insights into its therapeutic potential. Additionally, we evaluate the efficacy and safety of Ca in a $Tsc2^{-/-}$ subcutaneous tumor model, offering experimental evidence for its application in TSC-related diseases. Our findings not only elucidate

the molecular mechanisms underlying Ca's anti-tumor effects but also propose a novel therapeutic approach for managing Tsc2-associated lesions with potential implications for other mTOR-driven disorders.

Methods

Cell Line

Tsc2$^{+/+}$p53$^{-/-}$ and *Tsc2*$^{-/-}$p53$^{-/-}$ MEFs were the gift of David Kwiatkowski used under approved protocols (Jiangsu Province Institute of Traditional Chinese Medicine Ethics No. AEWC-20200520-108). *Tsc2*$^{-/-}$ and constitutive activation of mTORC1 were confirmed by immunoblotting of tuberin and phospho-S6, respectively. The novel *Tsc2*$^{-/-}$ cystadenoma cell line, 105K, was derived from a *Tsc2*$^{+/-}$ C57Bl/6 mouse renal tumor and isolated in the laboratory of Dr. Elizabeth Henske. These cells were confirmed to have loss of the second allele of *Tsc2* by PCR, loss of tuberin expression and increased phospho-S6 levels by immunoblotting. All cells were cultured in DMEM supplemented with 10% FBS, 100 μg/mL penicillin and 100 μg/mL streptomycin.

Crystal Violet Staining

Crystal violet was tested using a dedicated kit (C0121, Beyotime, China). In simple terms, after the cells are fixed, the staining solution is directly dropped in. After 10 minutes, they are thoroughly washed with distilled water for observation and photography.

Cell Viability Detection

The viability of *Tsc2*$^{-/-}$ cells was detected by the MTT method (n=6 per group). Briefly, 5×10^3 cells were seeded onto 96-well plates[19] and treated with indicated concentrations of Ca. After 24 h, 50 μL 1 × MTT solution (diluted by dilution buffer, KeyGENBioTECH) was added and incubated for 4h. Then, 150 μL DMSO was added. The absorbance at 470 nm was measured by the microplate reader.

Cell Cycle Analysis

Cell cycle progression was determined by propidium iodide (PI) staining and flow cytometry. Briefly, cells were harvested, resuspended, and fixed in pre-cooled 70% ice-cold ethanol at 4°C overnight. The cell suspension was then concentrated to a density of approximately 1×10^6 cells/mL in the fixation buffer to ensure a sufficient number of cells were present for analysis. Fixed cells were then treated with PI (50 μg/mL) and RNase A (100 μg/mL) for 60 minutes at room temperature. DNA fluorescence was monitored using a FACScan Flow Cytometry (BD FACSCalibur) with 10,000 events per determination, and data were analyzed using Modft LT program (Verity Software, UsA).

Quantitative Real-Time PCR

Total RNA was extracted using RNA-easy Isolation Reagent (R701-01, Vazyme, China) and reverse transcribed to cDNA using the HiScript IV 1st Strand cDNA Synthesis Kit (R412-01, Vazyme, China). qPCR was performed using ChamQ SYBR Color qPCR Master Mix (Q411-02, Vazyme, China).

Proteomic Detection and Analysis

We used a total of 8 samples (2 cases in the Blank group, 3 cases each in the h24 group and the h48 group) for proteomics analysis. After routine protein extraction and quantification, samples were submitted to LUMINGBIO (www.lumingbio.com; China) for testing. All raw data were subsequently analysed by R Studio and R-related software. We defined the proteins with p-value < 0.05 and a linear fold-change > 2 as inter-group difference proteins,[20] and other Comparison between groups was performed using the Student's t- test.

ATP Production Detection

ATP was quantified using an ATP assay kit (Beyotime, S0026) according to the manufacturer's protocols on a microplate reader (EnSpire, Perkin−Elmer, Singapore) (n = 3). In simple terms, after cell lysis, take an appropriate amount of ATP

detection reagent and dilute it with ATP detection reagent diluent at a ratio of 1:9. Add 100 microliters of ATP detection working solution to the detection hole. Let it stand at room temperature for 3 to 5 minutes to consume all the background ATP, thereby reducing the background. Add 20 microliters of sample or standard to the detection hole and determine the ATP content using a luminometer.

JC-1 Staining Protocol for Mitochondrial Membrane Potential (Δψm) Assay

Cells were incubated with 2–5 μM JC-1 (Thermo Fisher, T3168)[21] in culture medium at 37°C for 20–30 min. After washing with PBS, cells were analyzed by fluorescence microscopy/flow cytometry. For microscopy, red (ex/em: 540/590 nm) and green (485/535 nm) channels were acquired. Positive control: Cells treated with 10 μM CCCP (30 min) to induce ΔΨm collapse (reduced red/green ratio);Negative control: Unstained cells for autofluorescence correction).

Immunofluorescence

Cells were washed with PBS and fixed with 4% paraformaldehyde for 10 min at room temperature (RT), followed by permeabilization with 0.1% Triton X-100 for 5 min. After blocking with 5% normal goat serum (in PBS containing 0.3% Triton X-100) for 1 h at RT, samples were incubated overnight at 4°C with a rabbit monoclonal anti-KI67 antibody (SP6 clone, Abcam, #ab16667; 1:300 dilution in 1% BSA-PBS). The next day, cells were washed three times with PBS (5 min each) and incubated with Alexa Fluor 488-conjugated goat anti-rabbit IgG secondary antibody (Invitrogen, #A-11008; 1:500 dilution) for 1 h at RT in the dark. Nuclei were counterstained with DAPI (1 μg/mL, 5 min), and slides were mounted using ProLong Gold Antifade Mountant (Thermo Fisher). KI67-positive cells (green fluorescence) with DAPI (blue) labeling all nuclei. Cell fluorescence was visualized using the IXplore SpinSR (Olympus), while tissue fluorescence was scanned and analyzed using a Digital Slice Scanner (VS200, Olympus).

Animal Model Construction

8-week-old female BALB/cNj-Foxn1nu/Gpt mice were obtained from the Model Animal Research Center of Nanjing University (Nanjing, Jiangsu, China). All procedures were conducted in compliance with the Animal Care and Use Committee guidelines of the institution. Mice were housed under a 12-hour light/dark cycle with free access to food and water. For the subcutaneous model establishment, female nude mice were subcutaneously injected with 5×10^6 *Tsc2*$^{-/-}$ cells in right flank. At the same time mice were treated daily with physiological saline or 100 mg/kg/day or 200 mg/kg/day Canagliflozin via oral gavage for 20 days (n = 6). Tumor volumes were calculated according to the following formulation: Tumor volume = Length × Width^2 × 0.5. Animal weight was monitored and recorded.

H&E Staining

Tissue sections were routinely deparaffinised and then stained for nuclei using hematoxylin, cytoplasm was stained using matching eosin after a 30-second reaction in 0.25% ammonia, and finally the sections were sealed with neutral gum. Sections were scanned and analyzed in a Digital Slice Scanner (VS200, Olympus).

ALT, AST Measurement

Mouse serum or plasma was extracted and tested using special kits for ALT (C009-1-1) and AST (C010-1-1) from Nanjing Jiancheng Bioengineering Institute. All operations were performed according to the kit instructions. In simple terms, first add the matrix solution preheated at 37 degrees and the sample to be tested to the 96-well plate, react at 37 degrees for 30 minutes, then add 2, 4-dinitrophenylhydrazine, react at 37 degrees for 20 minutes, and then add 0.4 mol/L sodium hydroxide. After standing at room temperature for 15 minutes, the detection is carried out on a microplate reader with an appropriate wavelength.

BUN Measurement

Mouse serum or plasma was extracted and tested using special kits for BUN (C013-2-1) from Nanjing Jiancheng Bioengineering Institute. In simple terms, add 20 microliters of the sample to be tested and 250 microliters of buffer solution in sequence into a centrifuge tube. After a 10-minute water bath at 37 degrees, add 1mL of phenol chromogenic

reagent and 1mL of alkaline sodium hypochlorite respectively. After a 10-minute water bath at 37 degrees, draw 200 microliters of liquid into a 96-well plate and measure the absorbance at a wavelength of 640nm.

Statistical Analysis

Data are expressed as mean ± SEM. Comparison between groups was performed using the Student's *t* test or one-way ANOVA with the Holm-Sidak post-hoc test for multiple comparisons by using GraphPad Prism v10.0. A p-value < 0.05 was considered statistically significant. In addition, all experiments have undergone biological repetition to ensure their accuracy and reproducibility.

Results

Ca Inhibits Proliferation and Activity of Murine Tsc2$^{-/-}$ Cells

To assess the potential broad-spectrum efficacy of SGLT2 inhibitors on *Tsc2*$^{-/-}$ cells, we evaluated the antiproliferative effects of four SGLT2 inhibitors—canagliflozin (Ca), dapagliflozin, empagliflozin, and ertugliflozin—on *Tsc2*$^{-/-}$ cells. All the drugs were dissolved in DMSO. Dose-response experiments revealed that Ca exhibited the most pronounced antiproliferative activity, with significant inhibition observed at a concentration as low as 20 μM while we conducted MTT assay (Figure 1A). While dapagliflozin showed comparable activity at 20 μM (Figure 1B), its potency was markedly weaker than Ca at higher concentrations (Figure 1E). In contrast, empagliflozin and ertugliflozin had minimal effects on cell activity across all tested doses (Figure 1C and D), further underscoring the pharmacological advantage of Ca. The reduced crystal violet intensity suggests that CA significantly inhibits *Tsc2*$^{-/-}$ cell proliferation (Figure 1F). To quantify its potency, we determined the IC50 value of Ca for *Tsc2*$^{-/-}$ cells, which was 54.93 μM, indicating a robust inhibitory effect on proliferation (Figure 1G).Ca exhibited significantly less cytotoxicity in these control cell lines compared to *Tsc2*$^{-/-}$ MEFs. This indicates that the anti-proliferative effect of Ca observed in our study is not merely

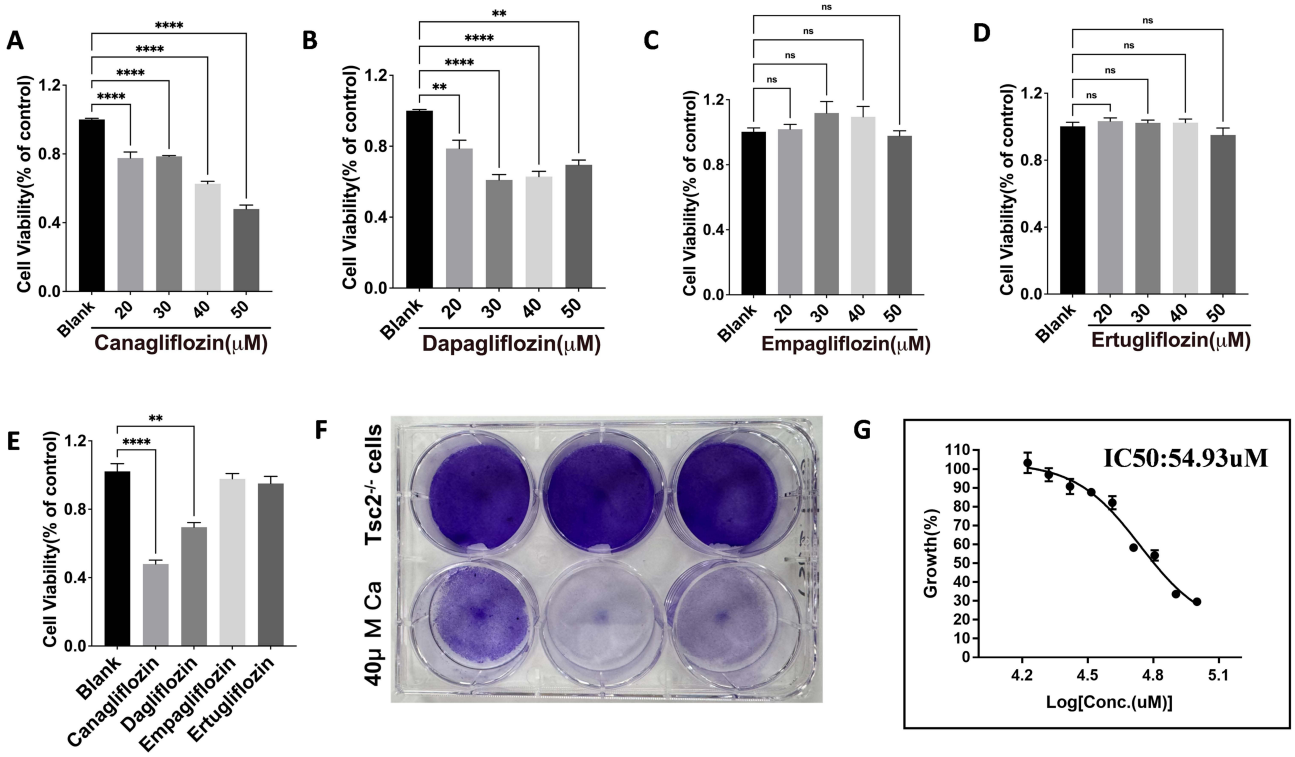

Figure 1 Effect of SGLT2 inhibitors on the viability and proliferation of mouse *Tsc2*$^{-/-}$ cell. (**A**) Canagliflozin inhibits the viability of *Tsc2*$^{-/-}$ cell in a concentration-dependent manner. Cells were treated with Canagliflozin (0–50μM) for 48 hours and detected by MTT assay. (**B**) Dapagliflozin inhibits the viability of *Tsc2*$^{-/-}$ cell. (**C** and **D**) Empagliflozin and Ertugliflozin do not alter *Tsc2*$^{-/-}$ cell viability. (**E**) Effect of 40μM SGLT2 inhibitors on the viability of *Tsc2*$^{-/-}$ cell. Results are mean ± SEM (n = 6). *, Statistically significant effect of SGLT2 inhibitors. (**F**) Crystal violet assay confirmed that canagliflozin inhibits proliferation of *Tsc2*$^{-/-}$ cell. (**G**) Plot of Canagliflozin concentration and *Tsc2*$^{-/-}$ cell growth density, with a probed IC50 value of 54.93uM."**" P<0.01, "****" P<0.0001, "ns" no significant difference.

https://doi.org/10.2147/DDDT.S525749

due to general toxicity but shows selectivity towards Tsc2-deficient cells. However, at the same time, Ca does exhibit a relatively narrow safety window: at a concentration of 100 μM, it inhibits the viability of both normal and mutant cells (Figure S1A). In addition, to further investigate the selectivity profile of Ca, we have also evaluated its effects in three other cancer cell lines: the hepatocellular carcinoma line HEPG2, and the gastric cancer lines MKN28 and AGS. Interestingly, at 50 μM, Ca promoted the growth of HEPG2 cells, while exerting varying degrees of inhibition in the gastric cancer cells (Figure S1B). These results collectively suggest that the pharmacological effects of Ca are independent of its general cytotoxic properties.

Ca Selectively Induces G1 Phase Arrest in Tsc2$^{-/-}$ Cells

To elucidate the mechanistic basis of Ca-induced growth suppression in *Tsc2*-deficient cells, we analyzed cell cycle dynamics in both *Tsc2*$^{+/+}$ and *Tsc2*$^{-/-}$ cells following 48 hours of Ca treatment. Initial assessments confirmed that Ca had no impact on the viability of *Tsc2*$^{+/+}$ cells, aligning with its selective activity against *Tsc2*$^{-/-}$ phenotypes (Figure 2A). Flow cytometry analysis revealed that untreated *Tsc2*$^{-/-}$ cells exhibited a higher proportion of cells in the S and G2 phases, indicative of active DNA replication and protein synthesis, as well as accelerated cell division. In contrast, Ca-treated *Tsc2*$^{-/-}$ cells displayed a significant accumulation in the G1 phase, suggesting a blockade in cell cycle progression and subsequent attenuation of proliferation and viability. Importantly, the cell cycle profile of *Tsc2*$^{+/+}$ cells remained unaltered upon Ca exposure, further corroborating its specificity for *Tsc2*$^{-/-}$ cells (Figure 2B and C).

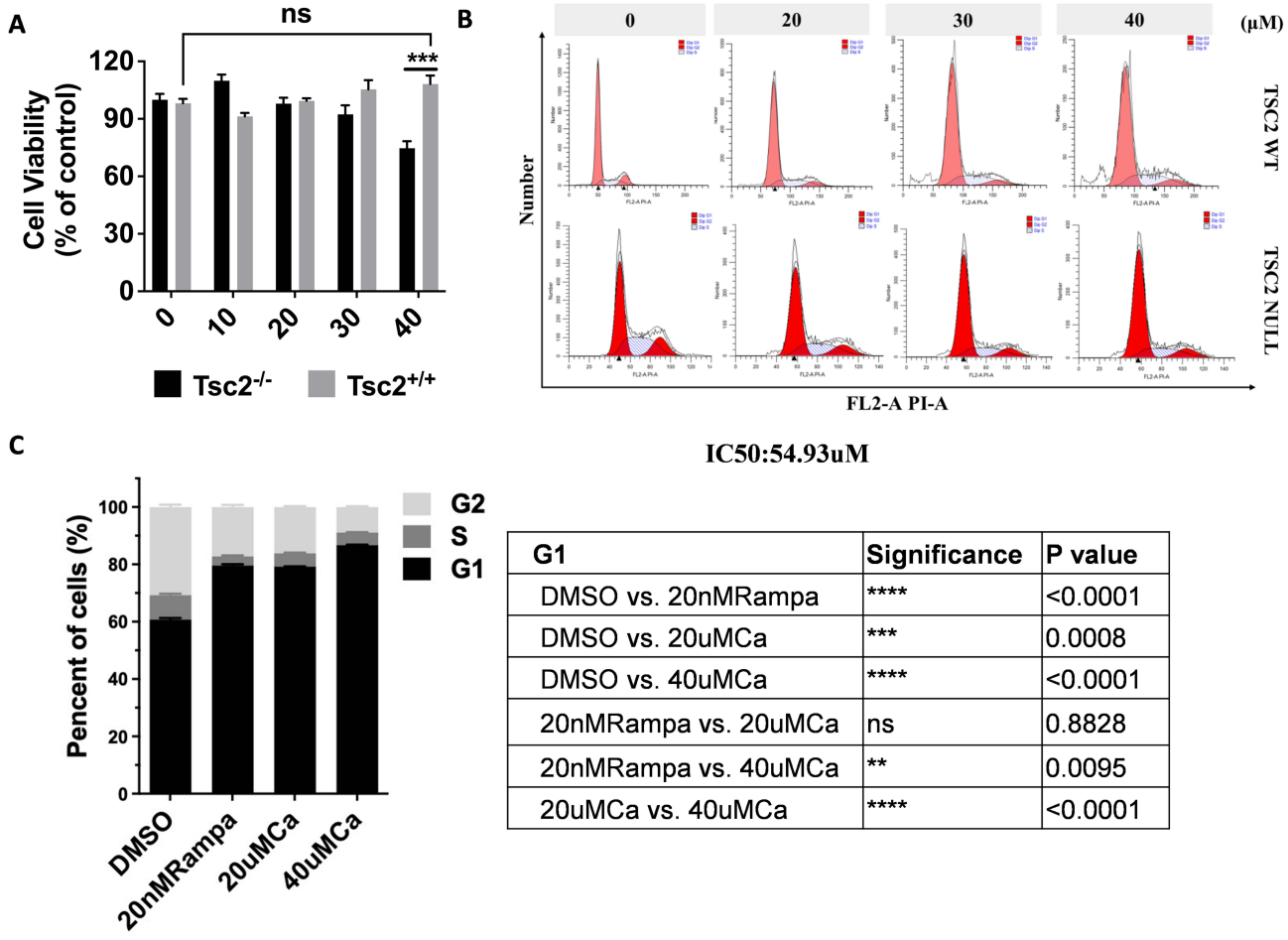

G1	Significance	P value
DMSO vs. 20nMRampa	****	<0.0001
DMSO vs. 20uMCa	***	0.0008
DMSO vs. 40uMCa	****	<0.0001
20nMRampa vs. 20uMCa	ns	0.8828
20nMRampa vs. 40uMCa	**	0.0095
20uMCa vs. 40uMCa	****	<0.0001

Figure 2 Canagliflozin selective inhibition of *Tsc2*$^{-/-}$ cell growth. (**A**) *Tsc2*$^{-/-}$ and *Tsc2*$^{+/+}$ cells were treated with different concentrations of canagliflozin, respectively, and cell viability results were then detected. (**B**) Cell cycle results of *Tsc2*$^{-/-}$ and *Tsc2*$^{+/+}$ cells after canagliflozin treatment were detected by flow cytometry. (**C**) Cell cycle statistics of *Tsc2*$^{-/-}$. "**" P<0.01, "***" P<0.001, "****" P<0.0001, "ns" no significant difference.

Proteomic Analysis Reveals Ca-Induced Alterations in Tsc2$^{-/-}$ Cell Protein Profiles

To further characterize the molecular mechanisms underlying Ca's effects on *Tsc2*$^{-/-}$ cells, we conducted proteomic profiling of untreated cells and those treated with Ca for 24 or 48 hours. Principal component analysis (PCA) revealed distinct clustering of protein expression profiles within each group, with clear separation between untreated and Ca-treated cells, as well as between the 24-hour and 48-hour treatment groups (Figure 3A). This robust separation underscores the significant temporal and treatment-dependent alterations in the proteome of *Tsc2*$^{-/-}$ cells induced by Ca.

Differentially expressed proteins (DEPs) were identified using stringent criteria (fold change ≥ 2 or ≤ 1/2, p-value < 0.05) (Table S1). Notably, the number of up-regulated proteins increased progressively with prolonged Ca treatment (Figure 3B). Venn diagram analysis highlighted the unique and shared DEPs across the three groups: 73 proteins (34.4% of total DEPs) were unique to the 24-hour treatment group, while 91 proteins (42.9% of total DEPs) were exclusive to the 48-hour treatment group (Figure 3C). This temporal divergence in protein expression further emphasizes the dynamic and sustained impact of Ca on *Tsc2*$^{-/-}$ cells, as also visualized in volcano plots (Figure 3D and E).

Gene Ontology (GO) analysis revealed that mitochondrial-associated proteins were significantly altered after 24 hours of Ca treatment, with further changes observed at 48 hours (Figure 3F and G). Among them, the key mitochondrial respiratory proteins Cyc2, Nduf7 and Atpb changed significantly (Figure 3I–K). Usually, exogenous Cyc2 cannot enter healthy cells. However, under hypoxia, the permeability of the cell membrane increases, and Cyc2 can enter cells and mitochondria. Figure 3I indicates that after Ca treatment, hypoxia in *Tsc2*$^{-/-}$ cells is obvious. Nduf7 and Atpb respectively reflect the dynamic changes of mitochondrial respiratory chain complexes I and V (Figure 3J and K), indicating that Ca can inhibit the function of respiratory chain complex I, resulting in a compensatory increase of respiratory chain complex V over time. These findings suggest that mitochondrial function is highly sensitive to Ca, potentially implicating impaired energy metabolism in the inhibition of *Tsc2*$^{-/-}$ cell proliferation and viability. In addition, Wikipathways enrichment analysis identified significant disturbances in the g1 to s cell cycle transition (Figure 3H), and the expression of E2f4 changed significantly (Figure 3L). This is a protein involved in cell cycle regulation or DNA replication and plays a role in controlling the process of the cell cycle from the G1 phase to the S phase. This result also confirms our earlier cell cycle results.

Ca Impairs Mitochondrial Function and Triggers Apoptosis in Tsc2$^{-/-}$ Cells

To assess the impact of Ca on mitochondrial function in *Tsc2*$^{-/-}$ cells, we employed JC-1 staining to evaluate mitochondrial membrane potential (ΔΨm). Following 40 μM Ca treatment, a significant reduction in J-aggregates (indicative of high ΔΨm) and a concomitant increase in J-monomers (indicative of low ΔΨm) were observed, suggesting a pronounced depolarization of the mitochondrial inner membrane (Figure 4A). Consistent with this finding, cellular ATP production was markedly suppressed by Ca treatment, further corroborating mitochondrial dysfunction (Figure 4B).

To identify specific alterations in the mitochondrial respiratory chain, we quantified the expression of key genes within complexes I–V. Notably, the expression of Ndufs2, a critical component of complex I, was significantly down-regulated, while Atp5o, a subunit of complex V, was upregulated (Figure 4C and D). These results suggest that Ca not only impairs ATP production but may also enhance cellular ATP consumption, possibly through compensatory mechanisms.

Given that mitochondrial depolarization is deeply related to the accumulation of reactive oxygen species (ROS), we then investigated ROS involvement in Ca-induced cell death. *Tsc2*$^{-/-}$ cells were loaded with 5 μM CM-H2DCFDA. Data represent fold-change vs untreated controls (mean ± SEM of 3 independent experiments). Using the CM-H2DCFDA fluorescent probe, we detected a 2.8-fold increase in ROS levels within *Tsc2*$^{-/-}$ cells after just 2 hours of Ca treatment (Figure 5A). Cells were pre-treated with 1 or 2 mM N-acetylcysteine (NAC) for 1 h. Viability was assessed at 24 h using Calcein-AM and normalized to untreated cells. One-way ANOVA with Tukey's post-hoc test. Strikingly, co-treatment with the ROS scavenger NAC restored cell viability to 85.3% ± 6.1% of the control group, compared to Ca treatment alone (Figure 5B and C). This rescue effect strongly implicates ROS as a critical mediator of Ca-induced cytotoxicity.

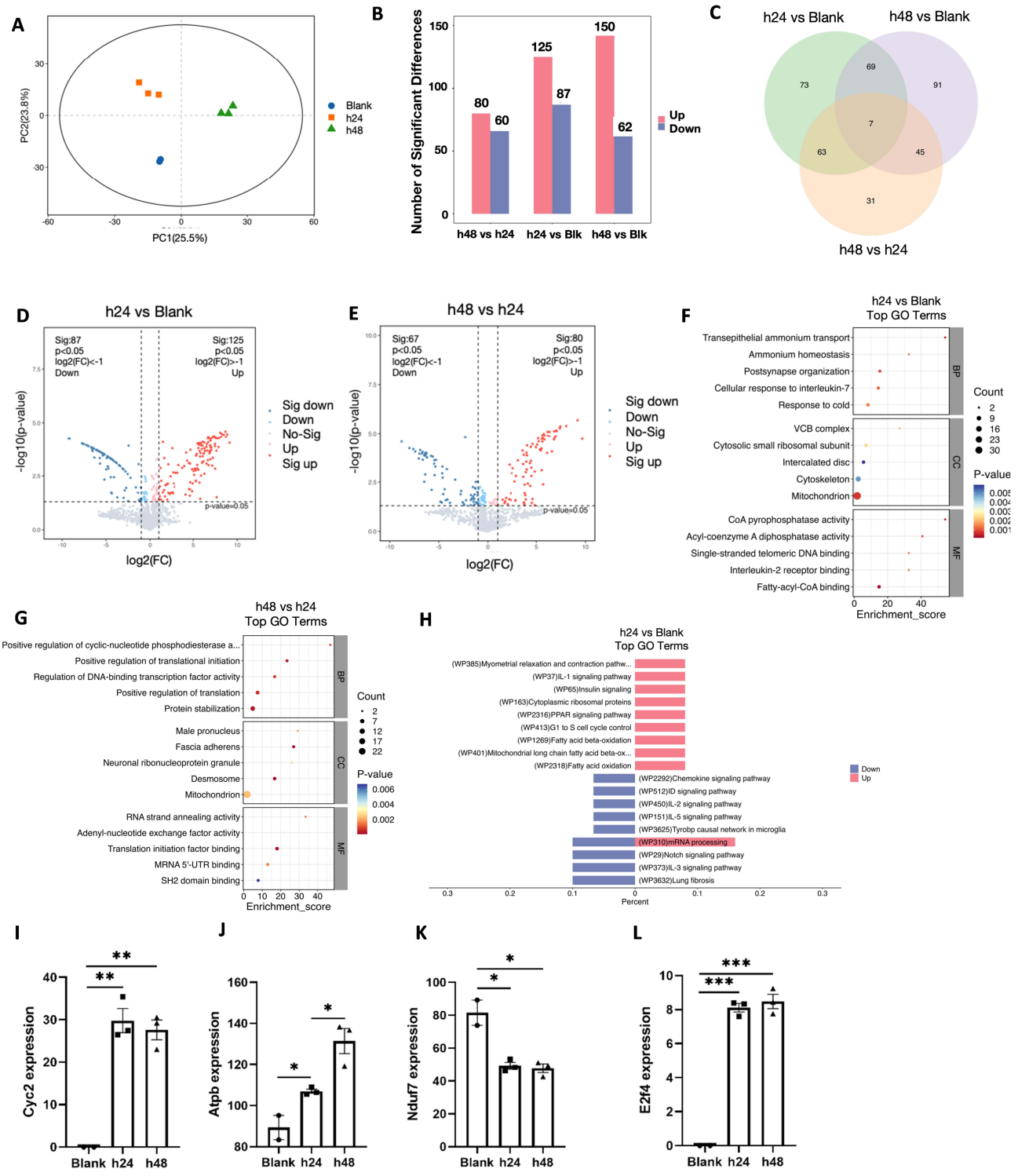

Figure 3 Proteomic results of canagliflozin treatment for 24 hours, 48 hours and control. (**A**) PCA principal component analysis showed significant differences in protein composition among the three groups. (**B**) Histogram statistics of differential proteins after two-by-two comparison of the three groups of data. (**C**) Venn diagram statistics for differential proteins. (**D**) Volcano plot showing the distribution of differential proteins between canagliflozin treatment for 24 hours and control group. (**E**) Volcano plot showing the distribution of differential proteins between canagliflozin treatment for 24 h and canagliflozin treatment for 48 h. (**F**) Differential analysis of top ranked GO entries between canagliflozin treatment for 24 h and control. (**G**) Differential analysis of top-ranked GO entries between canagliflozin-treated 24 h and canagliflozin-treated 48 h. (**H**) Comparison plot of up- and down-regulated pathways for Wikipathways enrichment analysis between canagliflozin treatment 24 h and control. (**I-L**) The expression patterns of Cyc2, Atpb, Nduf7 and E2f4 in the proteomics data. "*" P<0.05,"**" P<0.01, "***" P<0.001.

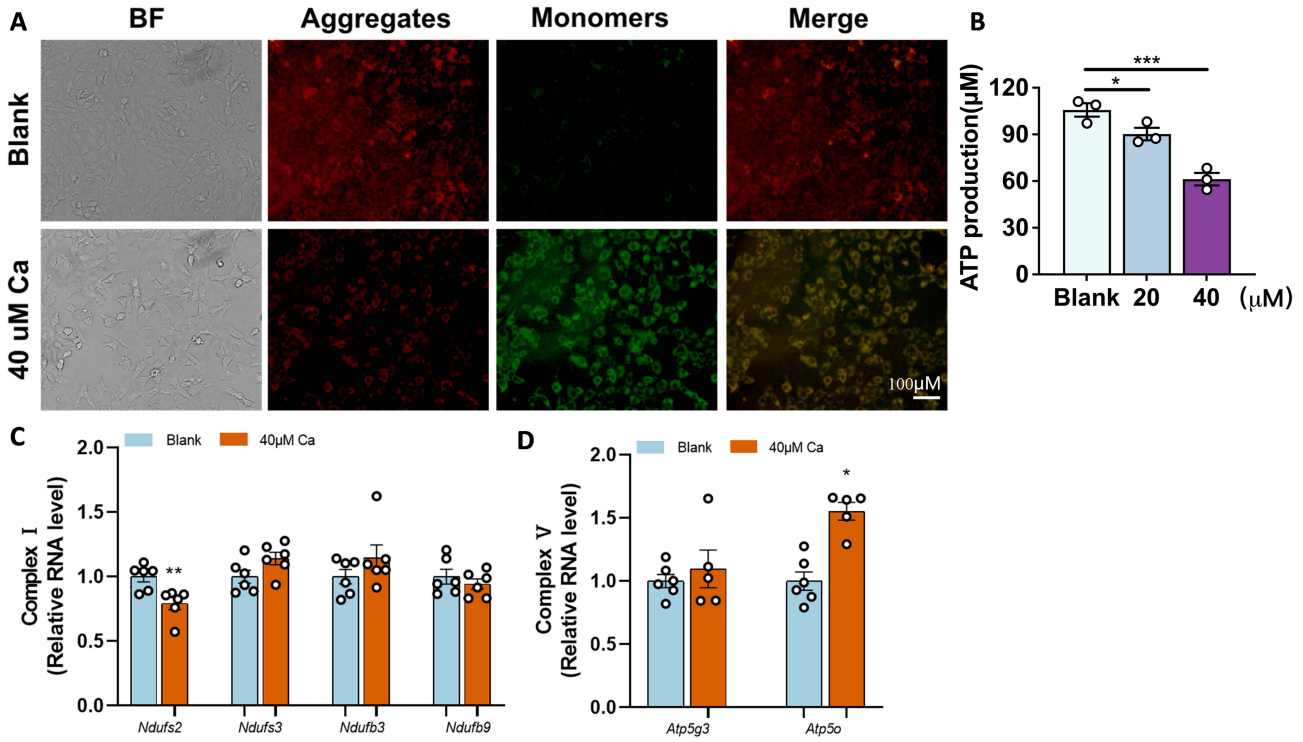

Figure 4 Detection of mitochondrial function and respiratory chain complex in *Tsc2*$^{-/-}$ cells after canagliflozin treatment. (**A**) JC-1 staining assay of mitochondrial inner membrane potential in *Tsc2*$^{-/-}$ cells before and after 40μM canagliflozin treatment. (**B**) Detection of ATP production after different doses of canagliflozin treatment in *Tsc2*$^{-/-}$ cells. (**C–D**) qPCR detection of mRNA expression of respiratory chain complex I–V markers. "*"P<0.05, "**" P<0.01, "***" P<0.001.

Ca Suppresses Tumor Growth in a Tsc2-/- Subcutaneous Mouse Model

To evaluate the antitumor efficacy of Ca in vivo, we established a subcutaneous tumor model in mice. Canagliflozin was prepared in normal saline. Experimental groups were administered Ca at doses of 100 mg/kg/day or 200 mg/kg/day via oral gavage for 20 days, while the control group received PBS. Ca treatment significantly reduced tumor volume in both dose groups, with no notable difference between the two (Figure 6A and B). However, mice treated with 200 mg/kg/day exhibited significant weight loss, likely attributable to drug-related side effects, whereas the 100 mg/kg/day group maintained body weight comparable to the control (Figure 6C). While our data demonstrate that 100 mg/kg/day produced effective, we acknowledge that future studies with additional dose tiers will be required to definitively establish the optimal dosage.

Histopathological analysis of tumor tissues harvested after 20 days of treatment revealed a marked reduction in tumor cell density following Ca administration, as evidenced by hematoxylin and eosin (HE) staining (Figure 6D). Furthermore, immunofluorescence staining demonstrated significant suppression of Ki67, a proliferation marker, in Ca-treated tumors, confirming the drug's antiproliferative effects (Figure 6E and F).

To assess potential organ toxicity, we measured serum levels of alanine aminotransferase (ALT), aspartate aminotransferase (AST), and blood urea nitrogen (BUN). Neither dose of Ca induced significant changes in these markers, indicating that oral administration of Ca is not hepatorenal toxic (Figure 6G–I). The mechanism underlying weight loss in the high-dose group remains to be elucidated and warrants further investigation.

In conclusion, this preclinical study indicates that Ca selectively targets *Tsc2*$^{-/-}$ cells through a dual mechanism: (1) Disrupting the cell growth cycle; (2) Induce mitochondrial dysfunction through excessive ROS production. Importantly, Ca exhibits strong anti-tumor activity and good safety in vivo, providing a strong preclinical theoretical basis for its treatment of TSC lesions. Of course, it is very necessary to conduct complete clinical trials and further molecular characterization before clinical application.

https://doi.org/10.2147/DDDT.S525749

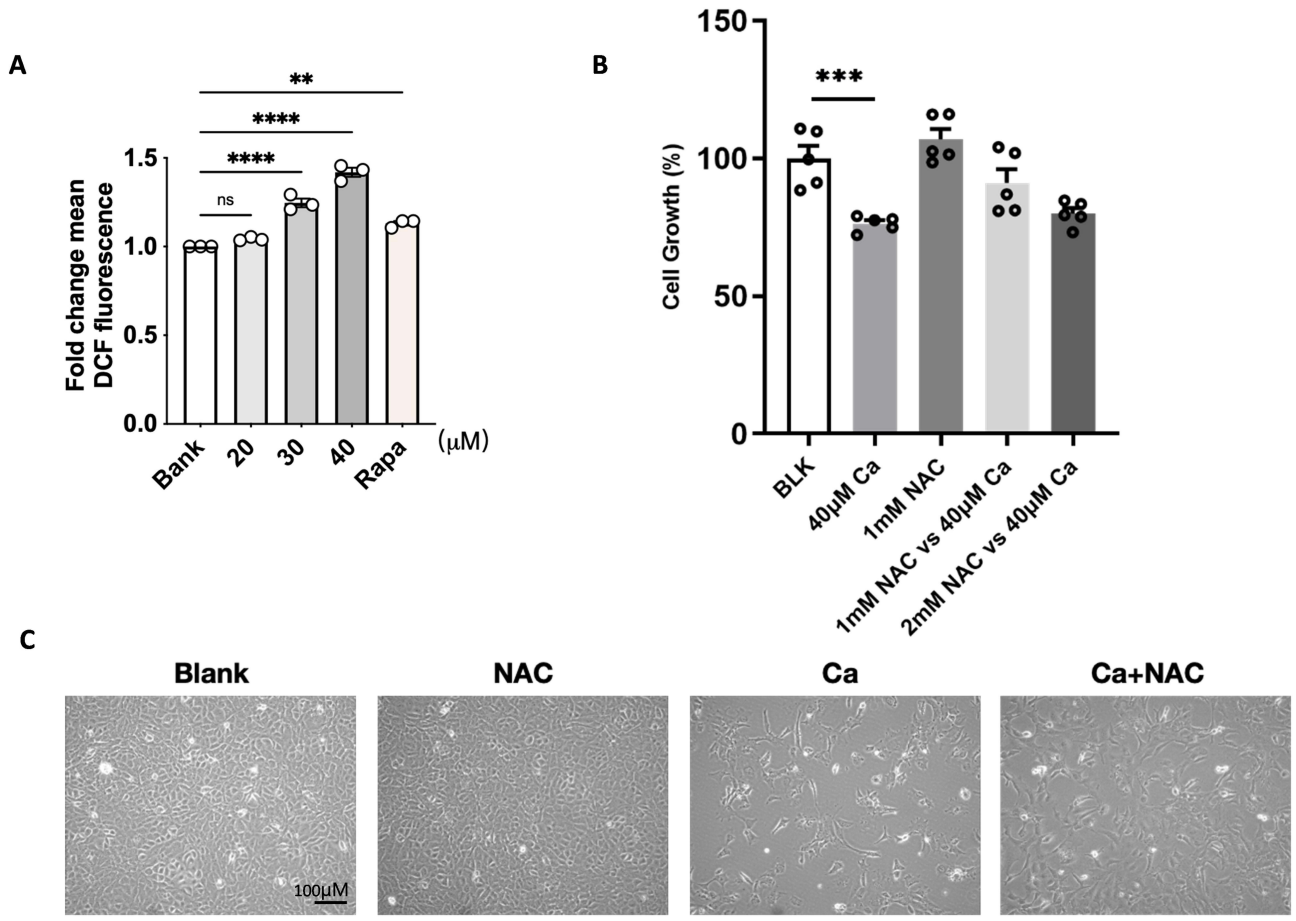

Figure 5 Detection of intracellular ROS production in *Tsc2*$^{-/-}$ cells and the effect of ROS on cell proliferation after different drug treatments. (**A**) Using the CM-H2DCFDA fluorescent probe assay to detect intracellular ROS production in *Tsc2*$^{-/-}$ cells. (**B** and **C**) Effects of ROS scavengers NAC (1mM) and 40μM Canagliflozin on *Tsc2*$^{-/-}$ cell growth. Statistical graphs (**B**) and microscopic views (**C**) are shown, respectively. "**" P<0.01, "***" P<0.001, "****" P<0.0001, "ns" no significant difference.

Discussion

Canagliflozin (Ca) was initially developed as a sodium-glucose cotransporter 2 (SGLT2) inhibitor to promote glucose excretion and lower blood glucose levels in patients with diabetes.[22] In recent years, its potential therapeutic applications in other diseases have attracted increasing attention. Beyond its well-established role in diabetes, Ca has shown efficacy in a variety of non-diabetes-related diseases, including non-small cell lung cancer (NSCLC),[12] pulmonary arterial hypertension,[23] and other lung pathologies.[24] Additionally, it has been effective against hepatocellular carcinoma (HCC),[25] glioblastoma (GBM),[26] and other tumors. In this preclinical study, we focused on TSC and demonstrated that canagliflozin has a significant inhibitory effect on the proliferation and activity of *Tsc2*$^{-/-}$ cells.

While Ca's primary mechanism as an SGLT2 inhibitor involves the suppression of glycolytic metabolism, including glucose uptake, lactate production, and intracellular ATP generation,[25] it also exerts SGLT2-independent effects on cell proliferation and migration. For instance, in HCC, Ca inhibits cancer cell proliferation by targeting the reduction of pyruvate kinase M2 (PKM2), thereby promoting the ubiquitination and degradation of the c-Myc oncogene.[27] Furthermore, under hypoxic conditions, Ca activates adenosine monophosphate-activated protein kinase (AMPK) and inhibits histone deacetylase 2 (HDAC2), leading to the downregulation of genes associated with the stability, metabolism, and survival of hypoxia-inducible factor-1α (HIF-1α). These effects collectively suppress the mTOR pathway, a key activator of HIF-1α signaling.[12] This multifaceted action likely contributes to Ca's potent inhibitory effects on target cells.

However, given the different clinical symptoms of TSC when it occurs in different tissues and organs, whether Ca is effective for all these clinical manifestations and whether off-target effects will occur still require more detailed subsequent studies. High aggregation of drugs in non-target organs or low aggregation in target organs can significantly

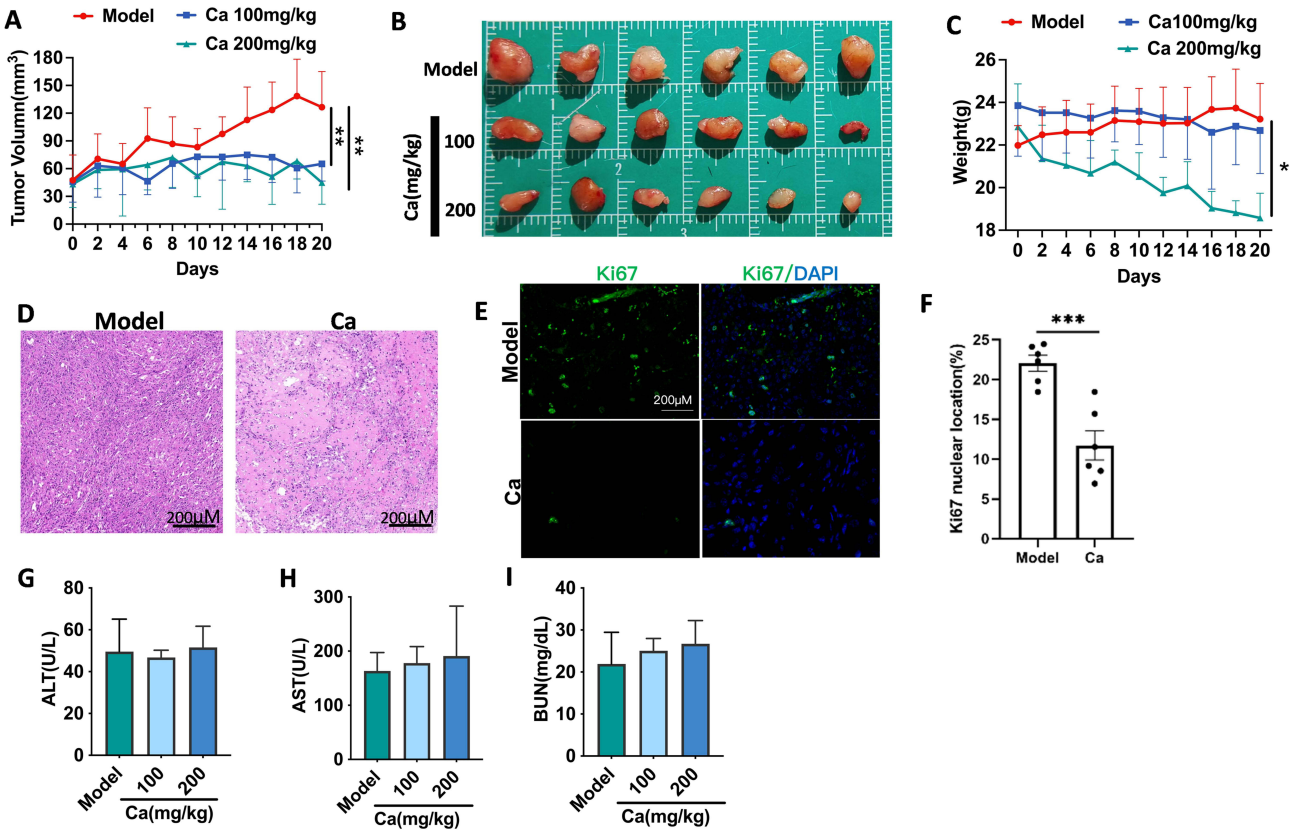

Figure 6 Canagliflozin exerts antitumor activity in *Tsc2*$^{-/-}$ cell subcutaneous tumor model. (**A**) Tumor growth in BALB/cNj-Foxn1nu/Gpt female mice with *Tsc2*$^{-/-}$ cells were administered daily by gavage by 100 mg/kg/day or 200 mg/kg/day Canagliflozin for 20 days (n=6). (**B**) The photograph of resected subcutaneous tumors that were explanted at the end of treatment period before sacrifice. (**C**) Body weights of BALB/cNj-Foxn1nu/Gpt female mice with *Tsc2*$^{-/-}$ cell tumors were subjected to 20-day treatment with placebo and Canagliflozin, respectively (n=6). (**D**) H&E staining of tumor of placebo- and Canagliflozin treated mice (n=6). Scar bar, 200 μm. (**E**) Immunofluorescence of Ki67 in the subcutaneous mice model. Scar bar, 200 μm (n=6). (**F**) Ki67 Immunofluorescence Staining Results Quantitative Statistics. (**G–I**): Canagliflozin administration did not alter the serum aspartate transaminase (AST), alanine aminotransferase (ALT) and blood urea nitrogen (BUN) level at the end of experiment. All data were presented as mean±SEM. Compared with the model, *P<0.05, ** P<0.01, *** P<0.001.

affect the safety and therapeutic efficacy of drugs, which is also a common cause of failure in the process of drug development and application. Subsequent studies may require the combination of Ca with different targeting strategies of small molecules, peptides or antibodies, and cells, and the selection of different strategies for clinical application. This tissue-specific drug delivery strategy has great potential in avoiding drug toxicity and can significantly improve the quality of life of patients.[28]

In this study, Ca demonstrated the best inhibitory effect on *Tsc2*$^{-/-}$ cells because other SGLT2 inhibitors, such as empagliflozin and dapagliflozin, did not show significant effects on the function of *Tsc2*$^{-/-}$ cells at low concentrations, while at high concentrations, their inhibitory effect on *Tsc2*$^{-/-}$ cells was not as excellent as that of Ca. This suggests that the anti-proliferative activity of Ca may be due to compound-specific mechanisms rather than a class-wide effect of SGLT2 inhibitors. The SGLT2-independent mechanisms described above may underlie the unique efficacy of Ca in targeting *Tsc2*$^{-/-}$ cells, and these pathways may also be relevant in TSC, providing a foundation for further investigation into the precise mechanisms of Ca in TSC treatment.

Our results also revealed that Ca treatment led to a significant reduction in the mitochondrial inner membrane potential of *Tsc2*$^{-/-}$ cells, an early indicator of apoptosis. Furthermore, we demonstrated the critical role of reactive oxygen species (ROS) in Ca's effects, as ROS scavenging abolished the anti-proliferative activity of Ca. However, the exact mechanism remains unclear. Previous studies have shown that Ca can promote mitochondrial oxidative metabolism in adipocytes by activating the AMPK-Sirt1-PGC1α signaling pathway,[11] which may transiently increase mitochondrial respiratory chain activity and ROS production.

https://doi.org/10.2147/DDDT.S525749

We also observed that Ca significantly reduced ATP production in *Tsc2*$^{-/-}$ cells, likely due to the reprogramming of energy metabolic pathways. Ca has been reported to reduce cellular dependence on glucose by inhibiting the mTOR pathway, shifting energy production toward fat oxidation.[29] Although fatty acid β-oxidation generates ATP, it is less efficient than glucose metabolism, potentially reducing overall ATP levels. Additionally, Ca-induced increases in ketone bodies (eg, β-hydroxybutyrate) may further inhibit ATP synthesis by suppressing mitochondrial complex I activity.[30] Moreover, Ca activation of the AMPK pathway, typically associated with energy stress, promotes catabolism while inhibiting anabolism, which may indirectly reduce ATP reserves.[31]

However, existing studies on ROS and ATP regulation by Ca present conflicting findings. For example, in models of vascular aging, Ca reduced aortic ROS levels.[32] Therefore, further research is needed to clarify the specific molecular targets and tissue-specific mechanisms of Ca in *Tsc2*$^{-/-}$ cells, as well as to assess the potential risks of energy metabolism imbalance during long-term treatment.

The *Tsc2* gene is a key regulator of the mTOR signaling pathway. Under normal circumstances, *Tsc2* inhibits mTOR, while mTOR regulates cell growth, proliferation, autophagy and protein-lipid synthesis. Conversely, *Tsc2* mutations lead to excessive activation of mTOR, which is a key factor in the pathogenesis of TSC.[33] Over the past five years, the FDA and EMA have approved several mTOR inhibitors, such as rapamycin, for the treatment of TSC.[8] However, its use is often associated with disease recurrence and serious side effects after drug withdrawal.[34] Recent studies have explored novel mTOR inhibitors, such as TC1, which targets both mTORC1 and mTORC2 signaling complexes. TC1 has shown promise in reducing seizure burden, prolonging survival in *Tsc2* hemizygous mice, and restoring developmental weight gain. However, its potential side effects after discontinuation remain unclear.[35] In this preclinical study, Ca demonstrated excellent anti-proliferative effects in *Tsc2*$^{-/-}$ cell without significant side effects or disease recurrence, suggesting its potential for clinical application. However, further studies in humans are needed to confirm these findings.

In vivo validation studies in mice demonstrated that oral administration of 100 mg/kg/day Ca achieved significant tumor suppression without notable adverse effects or metabolic toxicity. In contrast, mice treated with a higher dose of 200 mg/kg/day exhibited pronounced weight loss. The exact mechanism behind this phenomenon remains unclear. Studies have shown that classic hypoglycemic drugs, including Ca and metformin, can indeed reduce the weight, BMI, waist circumference and hip circumference of patients with insulin resistance.[36,37] Previous studies have proposed that Ca induces weight loss in patients with type 2 diabetes mellitus (T2DM) by inhibiting renal glucose reabsorption, enhancing lipolysis and fatty acid oxidation, and promoting adipose tissue browning.[38] Notably, one study found that the weight loss associated with Ca treatment was primarily attributable to a reduction in fat mass, rather than loss of muscle or other tissue volume.[39] However, a separate study highlighted a correlation between extreme weight loss induced by Ca and an increased risk of mortality.[40] Although the exact mechanism remains unclear, the weight loss induced by high-dose Ca is likely to involve a significant reduction in adipose tissue and may also lead to electrolyte imbalance in the body, an increased risk of fractures and muscle loss. In clinical practice, these risks can be effectively reduced by adhering to the standard dosing regimens prescribed by healthcare providers. We believe that subsequent studies need to comprehensively consider the use of Ca based on the BMI of patients with TSC. For TSC patients with a BMI ranging from 18.5 to 24, in addition to Ca treatment, protein intake should also be increased and regular impedance training should be carried out.[41,42] For patients with a BMI < 18.5 and elderly patients, perhaps Ca is no longer applicable. Of course, more in-depth systematic research is needed to verify our hypothesis.

Limitations

Despite promising results, our study has several limitations. First, the precise mechanisms by which Ca regulates ROS and ATP metabolism in *Tsc2*$^{-/-}$ cells remain unclear. Second, the potential for tissue-specific variations in Ca's effects requires further investigation. Third, while our in vivo studies demonstrated tumor suppression in mice, the translatability of these findings to human patients remains to be validated. Forth, Proteomics experiments are limited by the sample size and may have the problem of low statistical power.

Future Directions

Future studies should focus on elucidating the specific molecular targets of Ca in *Tsc2*$^{-/-}$ cells and assessing the risk of energy metabolism imbalance during long-term treatment. Additionally, comparative studies involving other SGLT2 inhibitors are needed to confirm Ca's unique effects. Further investigation into the role of ROS and ATP regulation in different tissues will provide a more comprehensive understanding of Ca's therapeutic potential. Finally, clinical trials are essential to evaluate Ca's efficacy and safety in human LAM patients.

Data Sharing Statement

Data sharing is not applicable to this article as no new data were created or analyzed in this study.

Ethics Statement

All procedures involving animals and cell lines were approved by the Institutional Animal Care and Use Committee of Affiliated Hospital of Integrated Traditional Chinese and Western Medicine, Nanjing University of Chinese Medicine and the details of the procedures were drafted in accordance with the guidelines. The experiment was conducted in accordance with the guidelines published by the National Institutes of Health.

No humans were involved in this study.

Acknowledgment

The research was supported by the Chinese National Science Foundation (32271187,3132071142,32300646,82104508); the Nature Science Foundation of Jiangsu Province (BK20230300); Medical research project of Jiangsu Provincial Health Commission (H2023103); Jiangsu Key Laboratory of Oral Diseases Research Open project fund (JSKLOD-KF -2303); Collaborative Innovation Center for Cancer Personalized Medicine - Clinical Research Fund of Hengrui Medicine (JZ21449020210617); The Basic Research Project of Changzhou Medical Center, Nanjing Medical University (CMCB202305); Natural Science Foundation of Xinjiang Uygur Autonomous Region (2023D01D05); Top innovative talent program of Nanjing Medical University (NJMUTY20230093); Youth Science and Technology Talent Support Project of Jiangsu Province (JSTJ-2024-102); High-level hospital science and technology innovation support plan application basic research project (KJCXQ2024012).

Author Contributions

Bin Xue, Juan Ye, Yinjuan Zhao and Jing Wu contributed to conception and manuscript design. Boyuan Liu drafted the manuscript. Juan Ye, Boyuan Liu, Hongliang Gao, Qingyun Wei and Kelei Su performed the experiments; Xuening Dai, Tao Xu, Yuqi Wang and Shuangchi Liu performed the data analysis. KaiZheng, Xing Peng and Liming Gou helped with manuscript preparation. Thanks to Kewei Lu that participated in the supplementary experiments for this study. All authors approved the final version of the manuscript for submission. All authors made a significant contribution to the work reported, whether that is in the conception, study design, execution, acquisition of data, analysis and interpretation, or in all these areas; took part in drafting, revising or critically reviewing the article; gave final approval of the version to be published; have agreed on the journal to which the article has been submitted; and agree to be accountable for all aspects of the work.

Funding

The study was funded by the Basic Research Program of Jiangsu (Grant No. BK20251969).

Disclosure

The authors have declared no competing interests.

References

1. Fu J, Liang P, Zheng Y, Xu C, Xiong F, Yang F. Corrigendum to "A large deletion in Tsc2 causes tuberous sclerosis complex by dysregulating PI3K_AKT_mTOR signaling pathway" (2024) 148312/D-23-04187]. *Gene*. 2024;919:148481. doi:10.1016/j.gene.2024.148481
2. Mizuguchi M, Ikeda H, Kagitani-Shimono K, et al. Everolimus for epilepsy and autism spectrum disorder in tuberous sclerosis complex: EXIST-3 substudy in Japan. *Brain Dev*. 2019;41(1):1–10. doi:10.1016/j.braindev.2018.07.003
3. Zhu QY, He ZM, Cao WM, Li B. The role of *Tsc2* in breast cancer: a literature review. *Front Oncol*. 2023;13:1188371. doi:10.3389/fonc.2023.1188371
4. Wheless JW, Wilson SML, Koenig MK, et al. Caregiver-reported nonseizure outcomes with real-world use of cannabidiol (CBD) in Tuberous Sclerosis Complex (TSC): interim results from the becometsc survey. *Ann Neurol*. 2025;96:S49–S49.
5. Curatolo P, Bombardieri R, Jozwiak ST. Tuberous sclerosis. *Lancet*. 2008;372(9639):657–668. doi:10.1016/S0140-6736(08)61279-9
6. McCormack FX, Inoue Y, Moss J, et al. Efficacy and safety of sirolimus in lymphangioleiomyomatosis. *N Engl J Med*. 2011;364(17):1595–1606. doi:10.1056/NEJMoa1100391
7. Crino PB, Nathanson KL, Henske EP. The tuberous sclerosis complex. *N Engl J Med*. 2006;355(13):1345–1356. doi:10.1056/NEJMra055323
8. Henske EP, Jóźwiak S, Kingswood JC, Sampson JR, Thiele, Thiele EA. Tuberous sclerosis complex. *Tuberous Sclerosis Complex Nat Rev Dis Primers*. 2016;2:16035. doi:10.1038/nrdp.2016.35
9. Song Y, Guo F, Liu Y, et al. Identification of circular RNAs and functional competing endogenous RNA networks in human proximal tubular epithelial cells treated with sodium-glucose cotransporter 2 inhibitor dapagliflozin in diabetic kidney disease. *Bioengineered*. 2022;13(2):3911–3929. doi:10.1080/21655979.2022.2031391
10. Ishibashi F, Kosaka A, Tavakoli M. Sodium glucose cotransporter-2 inhibitor protects against diabetic neuropathy and nephropathy in modestly controlled type 2 diabetes: follow-up study. *Front Endocrinol*. 2022;13:864332. doi:10.3389/fendo.2022.864332
11. Yang X, Liu Q, Li Y, et al. The diabetes medication canagliflozin promotes mitochondrial remodelling of adipocyte via the AMPK-Sirt1-Pgc-1α signalling pathway. *Adipocyte*. 2020;9(1):484–494. doi:10.1080/21623945.2020.1807850
12. Biziotis OD, Tsakiridis EE, Ali A, et al. Canagliflozin mediates tumor suppression alone and in combination with radiotherapy in non-small cell lung cancer (NSCLC) through inhibition of HIF-1α. *Mol Oncol*. 2023;17(11):2235–2256. doi:10.1002/1878-0261.13508
13. Wang S, Sui M, Chen Q, et al. Engineering PD-L1 targeted liposomal canagliflozin achieves multimodal synergistic cancer therapy. *Chem Eng J*. 2024:498
14. Behnammanesh G, Durante GL, Khanna YP, Peyton KJ, Durante W. Canagliflozin inhibits vascular smooth muscle cell proliferation and migration: role of heme oxygenase-1. *Redox Biol*. 2020;32:101527. doi:10.1016/j.redox.2020.101527
15. Yang C, Xiao C, Ding Z, Zhai X, Liu J, Yu M. Canagliflozin mitigates diabetic cardiomyopathy through enhanced pink1-parkin mitophagy. *Int J Mol Sci*. 2024;25(13):7008. doi:10.3390/ijms25137008
16. van Hameren G, Muradov J, Minarik A, et al. Mitochondrial dysfunction underlies impaired neurovascular coupling following traumatic brain injury. *Neurobiol Dis*. 2023;186:106269. doi:10.1016/j.nbd.2023.106269
17. Princen K, Van Dooren T, van Gorsel M, et al. Pharmacological modulation of septins restores calcium homeostasis and is neuroprotective in models of Alzheimer's disease. *Science*. 2024;384(6699):eadd6260. doi:10.1126/science.add6260
18. Zhang J, Kim J, Alexander A, et al. A tuberous sclerosis complex signalling node at the peroxisome regulates mTORC1 and autophagy in response to ROS. *Nat Cell Biol*. 2013;15(10):1186–1196. doi:10.1038/ncb2822
19. Xiaodan H, Lanqing H, Beibei X, et al. Activating STING/TBK1 suppresses tumor growth via degrading HPV16/18 E7 oncoproteins in cervical cancer. *Cell Death Differ*. 2023;31(1):78–89. DOI:10.1038/s41418-023-01242-w
20. Jürgen C, Matthias M. MaxQuant enables high peptide identification rates, individualized p.p.b.-range mass accuracies and proteome-wide protein quantification. *Nat Biotechnol*. 2008;26(12):1367–1372. doi:10.1038/nbt.1511
21. Smiley ST, Reers M, Mottola-Hartshorn C, et al. Intracellular heterogeneity in mitochondrial membrane potentials revealed by a J-aggregate-forming lipophilic cation JC-1. PNAS.1991. *Proceedings Nat Academy Sci United States Am*. 1991;88(9):3671–3675. doi:10.1073/pnas.88.9.3671
22. Ghezzi C, Yu AS, Hirayama BA, et al. Dapagliflozin binds specifically to sodium-glucose cotransporter 2 in the proximal renal tubule. *J Am Soc Nephrol*. 2017;28(3):802–810. doi:10.1681/ASN.2016050510
23. Tang L, Cai Q, Wang X, et al. Canagliflozin ameliorates hypobaric hypoxia-induced pulmonary arterial hypertension by inhibiting pulmonary arterial smooth muscle cell proliferation. *Clin Exp Hypertens*. 2023;45(1):2278205. doi:10.1080/10641963.2023.2278205
24. Lin F, Song C, Zeng Y, et al. Canagliflozin alleviates LPS-induced acute lung injury by modulating alveolar macrophage polarization. *Int Immunopharmacol*. 2020;88:106969. doi:10.1016/j.intimp.2020.106969
25. Kaji K, Nishimura N, Seki K, et al. Sodium glucose cotransporter 2 inhibitor canagliflozin attenuates liver cancer cell growth and angiogenic activity by inhibiting glucose uptake. *Int, J, Cancer*. 2018;142(8):1712–1722. doi:10.1002/ijc.31193
26. Shoda K, Tsuji S, Nakamura S, et al. Canagliflozin Inhibits Glioblastoma Growth and Proliferation by Activating AMPK. *Cell Mol Neurobiol*. 2023;43(2):879–892. doi:10.1007/s10571-022-01221-8
27. Zeng Y, Jiang H, Zhang X, et al. Canagliflozin reduces chemoresistance in hepatocellular carcinoma through PKM2-c-Myc complex-mediated glutamine starvation. *Free Radic Biol Med*. 2023;208:571–586. doi:10.1016/j.freeradbiomed.2023.09.006
28. Zhao Z, Ukidve A, Kim J, Mitragotri S. Targeting strategies for tissue-specific drug delivery. *Cell*. 2020;181(1):151–167. doi:10.1016/j.cell.2020.02.001
29. Osataphan S, Macchi C, Singhal G, et al. SGLT2 inhibition reprograms systemic metabolism via FGF21-dependent and -independent mechanisms. *JCI Insight*. 2019;4(5):e123130. doi:10.1172/jci.insight.123130
30. Eng TK, Elamir Y, Harrington M, Brito M. Euglycemic diabetic ketoacidosis associated with sodium-glucose cotransporter 2 inhibitor use and sars-cov-2: a case report. *J Gen Intern Med*. 2021;36:S328–S328.
31. Liu H, Chen W, Wan S, et al. Canagliflozin ameliorates high glucose-induced apoptosis in NRK-52E cells via inhibiting oxidative stress and activating AMPK/mTOR-mediated autophagy. *Mol Biol Rep*. 2023;50(12):10325–10337. doi:10.1007/s11033-023-08855-x
32. Wan F, He X, Xie W. Canagliflozin inhibits palmitic acid-induced vascular cell aging in vitro through ROS/ERK and Ferroptosis pathways. *Antioxidants*. 2024;13(7):831. doi:10.3390/antiox13070831

33. Nathan N, Wang JA, Li S, et al. Improvement of tuberous sclerosis complex (TSC) skin tumors during long-term treatment with oral sirolimus. *J Am Acad Dermatol*. 2015;73(5):802–808. doi:10.1016/j.jaad.2015.07.018
34. Cho JH, Patel B, Bonala S, et al. The Codon 72 TP53 polymorphism contributes to tsc tumorigenesis through the notch-nodal axis. *Mol Cancer Res*. 2019;17(8):1639–1651. doi:10.1158/1541-7786.MCR-18-1292
35. Dhamne SC, Modi ME, Gray A, et al. Seizure reduction in *Tsc2*-mutant mouse model by an mTOR catalytic inhibitor. *Ann Clin Transl Neurol*. 2023;10(10):1790–1801. doi:10.1002/acn3.51868
36. Kim YJ, Hwang SD, Lim S. Effects of sodium-glucose cotransporter inhibitor/glucagon-like peptide-1 receptor agonist add-on to insulin therapy on glucose homeostasis and body weight in patients with type 1 diabetes: a network meta-analysis. *Front Endocrinol*. 2020;11:553. doi:10.3389/fendo.2020.00553
37. Gong Z, Aragaki AK, Chlebowski RT, et al. Diabetes, metformin and incidence of and death from invasive cancer in postmenopausal women: results from the women's health initiative. *Int, J, Cancer*. 2016;138(8):1915–1927. doi:10.1002/ijc.29944
38. Ali AM, Martinez R, Al-Jobori H, et al. Combination therapy with canagliflozin plus liraglutide exerts additive effect on weight loss, but not on hba1c, in patients with type 2 diabetes. *Diabetes Care*. 2020;43(6):1234–1241. doi:10.2337/dc18-2460
39. Zheng H, Liu M, Li S, et al. Sodium-glucose co-transporter-2 inhibitors in non-diabetic adults with overweight or obesity: a systematic review and meta-analysis. *Front Endocrinol*. 2021;12:706914. doi:10.3389/fendo.2021.706914
40. Ferrannini G, Pollock C, Natali A, Yavin Y, Mahaffey KW, Ferrannini E. Extremes of both weight gain and weight loss are associated with increased incidence of heart failure and cardiovascular death: evidence from the CANVAS Program and CREDENCE. *Cardiovasc Diabetol*. 2023;22(1):100. doi:10.1186/s12933-023-01832-5
41. Kramer CK, Zinman B. Sodium-glucose cotransporter-2 (SGLT-2) inhibitors and the treatment of type 2 diabetes. *Annu Rev Med*. 2019;70:323–334. doi:10.1146/annurev-med-042017-094221
42. Pereira MJ, Eriksson JW. Emerging role of SGLT-2 inhibitors for the treatment of obesity. *Drugs*. 2019;79(3):219–230. doi:10.1007/s40265-019-1057-0